

# Improved CMB Map from WMAP Data

Hao Liu<sup>1\*</sup> and Ti-Pei Li<sup>1,2†</sup>

<sup>1</sup>*Key Laboratory of Particle Astrophysics, Institute of High Energy Physics, Chinese Academy of Sciences, Beijing, China*

<sup>2</sup>*Center for Astrophysics, Tsinghua University, Beijing, China*

## ABSTRACT

The cosmic microwave background (CMB) temperature maps published by the Wilkinson Microwave Anisotropy Probe (WMAP) team are found to be inconsistent with the differential time-ordered data (TOD), from which the maps are reconstructed. The inconsistency indicates that there is a serious problem in the map making routine of the WMAP team, and it is necessary to reprocess the WMAP data. We develop a self-consistent software package of map-making and power spectrum estimation independently of the WMAP team. Our software passes a variety of tests. New CMB maps are then reconstructed, which are significantly different from the official WMAP maps. In the new maps, the inconsistency disappeared, along with the hitherto unexplained high level alignment between the CMB quadrupole and octopole components detected in released WMAP maps. An improved CMB cross-power spectrum is then derived from the new maps which better agrees with that of BOOMRANG. Two important results are hence obtained: the CMB quadrupole drops to nearly zero, and the power in multiple moment range between 200 and 675 decreases on average by about 13%, causing the best-fit cosmological parameters to change considerably, e.g., the total matter density increases from 0.26 up to 0.32 and the dark energy density decreases from 0.74 down to 0.68. These new parameters match with improved accuracy those of other independent experiments. Our results indicate that there is still room for significant revision in the cosmological model parameters.

**Key words:** cosmic microwave background — cosmology: observations — cosmological parameters — early universe

## 1 INTRODUCTION

The CMB data from the WMAP mission is the most important basis of cosmology study, and the accuracies of the CMB map recovered from the WMAP data and its angular power spectrum are essential for precision cosmology.

Recently, we find there notably exist observational effects on released WMAP maps. The WMAP mission measures temperature differences between sky points using differential radiometers consisting of plus-horn and minus-horn (Bennett et al. 2003a). When an antenna horn points to a sky pixel, the other one will scan a ring in the sky with angular radius  $141^\circ$  to the center pixel. These measured TOD are transformed into the full-sky temperature anisotropy map by a map-making process (Hinshaw et al. 2003a). In released five-year WMAP (WMAP5) CMB maps we find significant distortion from hot Galactic sources: the pixels in the scan ring of a hot pixel are systematically cooled, and strongest anti-correlations between temperatures of a hot pixel and its scan-ring appear at a separation angle  $\theta \sim 141^\circ$  (Liu & Li 2009). The above results are confirmed by Aurich, Lustig & Steiner (2009). Furthermore, we also detect the no-negligible effect of imbalance observations in

published WMAP5 maps (Li et al 2009): systematical dependence of temperature vs. observation number difference between the two horns of a radiometer produced by the input transmission imbalance, and significant correlation between pixel temperature and observation number in WMAP data. These recent findings of systematical error in published WMAP temperature maps push us forward to further check the WMAP map-making processing.

In this work, we find a remarkable inconsistency between the WMAP TOD and published temperature map, which is described in §2. The revealed inconsistency demonstrates that there certainly exists a serious problem in WMAP map-making process, and it is worth to check the reliability of released WMAP results by reproducing CMB temperature maps from the original raw data independently from the WMAP team. We built a self-consistent software package of map-making from TOD and power spectrum estimation from reconstructed CMB maps. Our software successfully passes a variety of tests, i.e. the residual TOD test, the residual dipole component test, the map-making convergence test and the end-to-end test, which are presented in §3. With our software, improved CMB maps from WMAP TOD are produced and shown in §4, and the new angular power spectrum is derived from our new CMB maps and shown in §5. From the new angular power spectrum, we de-

\* E-mail: liuhao@ihep.ac.cn

† E-mail: litp@tsinghua.edu.cn

termine the new best-fit cosmological parameters and present the results in §6. Finally, we give a brief discussion of our results in §7.

## 2 INCONSISTENCY BETWEEN TOD AND RELEASED MAP

Let  $t_i$  denotes the temperature anisotropy at a sky pixel  $i$ . In a certain band, the observed difference of the  $k$ th observation  $d_k = t_{k^+} - t_{k^-}$ , where  $k^+$  and  $k^-$  are the sky pixels pointed by the plus-horn and minus-horn during the observation  $k$  respectively. From total  $L$  observations, the differential TOD

$$\mathbf{d} = \mathbf{A} \mathbf{t} \quad (1)$$

with  $\mathbf{A} = \{a(k, i)\}$  being the scan matrix. The most of elements  $a(k, i) = 0$  except for  $a(k, i = k^+) = 1$  and  $a(k, i = k^-) = -1$ . The WMAP team produces the released temperature map  $\hat{\mathbf{t}}$  from the calibrated TOD  $\mathbf{d}$  by using their map-making software (Hinshaw et al. 2003a; Jarosik et al. 2007).

Here we use a simple method to test the consistency between the WMAP TOD  $\mathbf{d}$  and the released map  $\hat{\mathbf{t}}$  reconstructed from  $\mathbf{d}$  by map-making. We calculate for each observation  $k$  the residual  $d'_k$  between the measured calibrated difference and the calibrated difference predicted by the reconstructed map,  $d'_k = d_k - (\hat{t}_{k^+} - \hat{t}_{k^-})$ , to get the residual TOD

$$\mathbf{d}' = \mathbf{d} - (\hat{\mathbf{t}}_+ - \hat{\mathbf{t}}_-). \quad (2)$$

If the temperature map is properly reconstructed, only the instrument noise should be left in  $\mathbf{d}'$ . To check it, we produce the correlation map of the residual TOD

$$\mathbf{t}_0 = \mathbf{M}^{-1} \mathbf{A}^T \mathbf{d}', \quad (3)$$

where  $\mathbf{M} = \mathbf{A}^T \mathbf{A}$  is diagonally dominant (Hinshaw et al. 2003a)

$$M^{-1}(i, j) \simeq \frac{1}{N_i} \delta_{ij} \quad (4)$$

with  $N_i$  being the total number of observations for pixel  $i$ . If the temperature map published by the WMAP team is reconstructed correctly, the correlation map  $\mathbf{t}_0$  should remain only the map-making error with low amplitude and no significant structured signal on it. Because Eq. 3 is linear, we have  $\mathbf{t}_0 = \mathbf{M}^{-1} \mathbf{A}^T \mathbf{d} - \mathbf{M}^{-1} \mathbf{A}^T (\hat{\mathbf{t}}_+ - \hat{\mathbf{t}}_-)$ . For a correctly reconstructed map  $\hat{\mathbf{t}}$ , both  $\mathbf{M}^{-1} \mathbf{A}^T \mathbf{d}$  and  $\mathbf{M}^{-1} \mathbf{A}^T (\hat{\mathbf{t}}_+ - \hat{\mathbf{t}}_-)$  will be equal to  $\hat{\mathbf{t}}$ , then  $\mathbf{t}_0$  will be exactly zero, despite the inevitable numerical computation error, or the map making error.

Now we check the consistency of released temperature map with the used WMAP TOD. In map-making, not all measured TOD are used by the WMAP team. During the preprocess of map-making, bit-coded quality flags are set (Limon et al. 2008). A non-zero flag indicates that either the observation is problematic in a specific respect, or the beam boresight is away from one of the out planets no more than  $7^\circ$ , which is the antennae main beam radius limit (Hill et al. 2009). In both cases, the corresponding data are at least less optimal, and some of these data (not all) are not used by the WMAP team in the map-making. We follow the WMAP team's flagging convention<sup>1</sup> to get the used WMAP5 year-1 TOD.

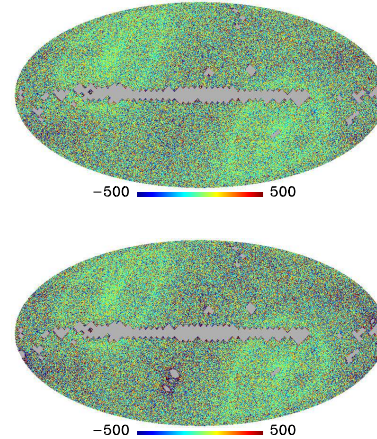


**Figure 1.** Correlation maps of residual TOD  $\mathbf{d}'$  between the input TOD and the TOD predicted by the official WMAP5 year-1 temperature map of Q1-band, in Galactic coordinates and in units of  $\mu\text{K}$ . The gray area represents pixels without valid value. *Upper panel:* The data used in map making are those used by the WMAP team to produce the released map. *Lower panel:* The data used in map making are the measured calibrated TOD of safe-mode. In this mode, less data are used, see text for details of this mode.

The upper panel of Fig. 1 shows the map  $\mathbf{t}_0$  obtained by Eq. 3 from the used WMAP5 year-1 TOD and the released WMAP5 year-1 temperatures of Q1-band, where visible structures along the ecliptic plane and around the ecliptic poles left and the rms amplitude  $\sim 265 \mu\text{K}$ , which is much higher than the expected rms error of  $\sim 0.2 \mu\text{K}$  estimated by the WMAP team with flight-like simulations for their map-making algorithm (Hinshaw et al. 2003a).

More than 95% of doubtful TOD data are non-zero flagged for the Sun, Earth, Moon and planet avoidance, the beam boresight angle for one of the planets is less than  $7^\circ$ . However, the criterion really used for the maps released by the WMAP team is a cut of only  $1^\circ.5$  (Limon et al. 2008), the revealed structure in the residual TOD may come from ecliptic contamination by used non-zero flagged TOD. To test this guess, we use only the high quality data whose quality flags are all zero (we call this the "safe-mode") to produce the residual TOD and its correlation map  $\mathbf{t}_0$ . The high quality TOD (all flags being zero) preserve more than 74% of all measured WMAP TOD, and the sky coverage of these data is more than 99.7% (neglecting the WMAP5 processing mask region). Therefore, these data in safe-mode not only can better avoid the contamination from the ecliptic plane, but also are enough to reconstruct a reliable CMB map as well. This is also ensured by an end-to-end test upon the total map-making and power-spectrum estimation processes shown in §3.4, where they are proved to be unbiased and highly accurate. The  $\mathbf{t}_0$  map from the safe-mode TOD, shown in the lower panel of Fig. 1, still remains a structure similar with what from the WMAP team used TOD and a large rms amplitude  $\sim 291 \mu\text{K}$ .

The above results of residual TOD test demonstrate there certainly exists a remarkable problem in the WMAP map-making pro-

<sup>1</sup> (1) GENERAL FLAG – Test on bits 0, 1, 3, 4, 5. This discards data when the observatory is not in observing mode, the Sun is visible over the shield, but included data when either the Earth or Moon are visible over the shield (but still in the far sidelobes of the radiometer beams). (2) DA-SPECIFIC FLAGS – Test on bit 0, re-test on bits 1–10. Bit 0 allows exclusion of data

with known thermal disturbances or radiometer upsets. Bits 1–10 show that a planet is close to a radiometer beam. If bit 1–10 is set, compute the distance between the indicated planet and the radiometer beam center based on the instantaneous pointings for all points within the frame, and discard only those points for which the planet lies within  $1^\circ.5$  of the beam.

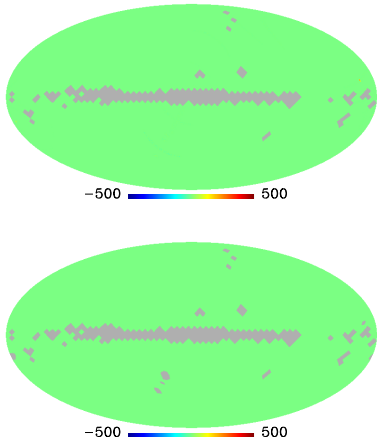


**Figure 2.** Correlation map of residual TOD between the input TOD and the TOD predicted by our new temperature map of Q1-band, in Galactic coordinates and in units of  $\mu\text{K}$ . The gray area represents pixels without valid value. *Upper panel:* The data used in map making are those used by the WMAP team to produce the released map. *Lower panel:* The data used in map making are the measured calibrated TOD of safe-mode. In this mode, less data are used, see text for details of this mode.

cess and using carefully tested software to improve the previous released WMAP results is really needed.

### 3 SOFTWARE TESTING

We write out our programs for map-making and power spectrum estimation. The input of our map-making program is the calibrated TOD (Limon et al. 2008) downloaded from the WMAP team’s website ([ftp://lambda.gsfc.nasa.gov/](http://lambda.gsfc.nasa.gov/)). According to the WMAP document (Hinshaw et al. 2003a), only three extra corrections are needed: the  $1/f$  noise removal, the sidelobe correction, and the transmission imbalance correction. The sidelobe correction is applied only to the K-band, and other two corrections are applied to all bands. To check the reliability of released WMAP results by reproducing CMB maps from the original raw data independently, firstly we must test our map making and power spectrum estimation softwares to make sure that they produce correct outputs. This includes four tests: the residual TOD test, the residual dipole component test, the map-making convergence test, and, finally, the end-to-end test checking all our data pipeline in a self-consistent manner.

#### 3.1 Residual TOD

With our map-making program we produce new temperature map, and with the new map and Eq. 3 we calculate the residual TOD as already illustrated. All these are done for both the WMAP5 year-1 Q1-band TOD and the corresponding safe-mode TOD separately, and their correlation maps are shown in the upper and lower panels of Fig. 2 respectively. In both maps, no significant structure can be seen and the rms amplitudes are all less than  $0.15 \mu\text{K}$ , almost 2000 times lower than what from the WMAP team’s map-making products and close to the rms error of  $\sim 0.11 \mu\text{K}$  of our map-making (see §3.3), indicating the inconsistent problem presented in §2 is prevented in our map-making algorithm.

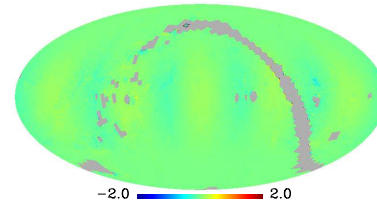


**Figure 3.** Map-making error,  $t_{out} - t_{in}$  ( $\mu\text{K}$ ), in ecliptic coordinates by our map-making software after 50 rounds of iterations. The input map is Q1-band WMAP5 temperature map without foreground removal, and the map-making is done with our software in safe-mode. All observations with either beam inside the WMAP5 processing mask are rejected in addition to the safe-mode data rejection. The rms of  $t_{out} - t_{in}$  in this map is  $\sim 0.11 \mu\text{K}$ . The gray area represents pixels without valid value.

It has to be noted that we repeat the map making by writing our own code but following every step given by the WMAP document (Hinshaw et al. 2003a), but do not encounter their problems in our output maps. This demonstrates that the method of WMAP map-making could in principle succeed in recovering temperature maps, but in practice the WMAP team do not implement their own method correctly.

#### 3.2 Residual Dipole Component

The filtered calibrated TOD can not be directly used for map-making, because they contain large dipole component caused by the joint motion of the sun and the satellite. This dipole component is subtracted according to the WMAP team’s literature (Hinshaw et al. 2008, §4). After subtracting the unwanted dipole component, the residual dipole component amplitude outside the KQ85 mask in our Q1-band map is estimated to be  $7.56 \mu\text{K}$  and point to the Galactic coordinates  $(13^\circ.16, -11^\circ.78)$ . Meanwhile, the residual dipole component amplitude outside the KQ85 mask in the Q1-band WMAP5 official map is also estimated, which is  $7.92 \mu\text{K}$  and points to the Galactic coordinates  $(3^\circ.93, -14^\circ.70)$ . Both these dipole components are estimated with the “remove\_dipole” program from the standard HEALPix package (Gorski et al. 2005), and the difference between them is about  $1.1 \mu\text{K}$ . Since the original dipole component amplitude is several hundreds times larger than the residual dipole, the neglectable difference between the two residual dipole components derived from the new and old CMB maps indicates that both our map-making and dipole component removal have high accuracy and their results are reliable.

#### 3.3 Convergence of Map-making Algorithm

The map-making algorithm is an iterative one, thus it is important to test its convergence. An official test had been adopted by the WMAP team (Hinshaw et al. 2003a). They generated artificial TOD from simulated CMB map ( $t_{in}$ ) according to the scan scheme of the real observations, then use the artificial TOD to do map-making and compare the result  $t_{out}$  with  $t_{in}$  to see if their software converges well. The output  $t_{out}$  is expected to be very close to the known input  $t_{in}$ , and the rms of  $t_{out} - t_{in}$  is expected to decrease as the number of iterations increases, right as presented in the WMAP team’s literature (Hinshaw et al. 2003a, Fig. 2, 50 rounds of iterations).

We repeat this test with our map-making software for four individual tests: (1)  $t_{in}$  being real WMAP temperature maps and

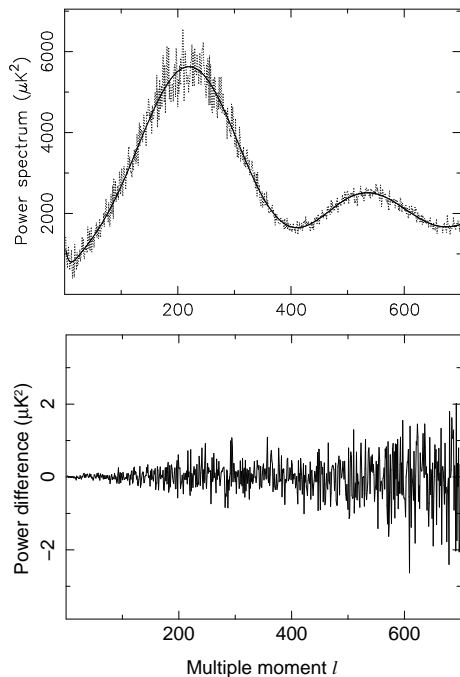


**Figure 4.** End-to-end test. *Upper panel:* the input  $\Lambda\text{CDM}$  power spectrum (solid line) and the final cross power spectrum (dotted line). *Lower panel:* power differences between the final cross-power spectrum and the cross power spectrum generated by synfast,  $C_{final} - C_{synfast}$ .

the scan scheme being safe-mode; (2) similar to the above test but the scan scheme being all observations; (3) and (4) are similar to (1) and (2) respectively, but  $t_{in}$  being simulated CMB maps plus WMAP-like foreground. Each test was run for 50 rounds of iterations. Theoretically speaking, the results of these four tests should be very close to each other, because the inputs and map-making environments do not differ much among them. The test results are right as expected: The maps of  $t_{out} - t_{in}$  given by all the four tests are similar to the WMAP team’s official test (Hinshaw et al. 2003a, Fig. 2), and all the four rms of  $t_{out} - t_{in}$  are less than  $0.2 \mu\text{K}$ , which do not exceed the residual rms given by the WMAP team. The result of test (1) for Q1-band is presented in Fig. 3. The results of tests (2)–(4) are similar to Fig. 3. With such tests, we are confident that our software is able to make reliable CMB maps from the WMAP TOD.

### 3.4 End-to-End Test

This is the most important test, in which the overall map-making and power spectrum estimation are checked in an end-to-end way: starting from the best-fit WMAP5  $\Lambda\text{CDM}$  power spectrum ( $C_{\Lambda\text{CDM}}$ ), we use the “synfast” routine in HEALPix software package (available at <http://healpix.jpl.nasa.gov>) to generate simulated sky maps for V and W-bands, and then use these maps to produce artificial TOD in safe-mode. These artificial TOD are used to do map-making and then the recovered maps by the map-making process are used to compute the final cross-power spectrum ( $C_{final}$ ). In the end,  $C_{final}$  is compared to  $C_{\Lambda\text{CDM}}$  to finish the end-to-end test.

Such a test can definitely illustrate two things: whether the  $\sim 74\%$  observations used in map-making are enough to recover an unbiased CMB map, and whether our data pipeline is unbiased

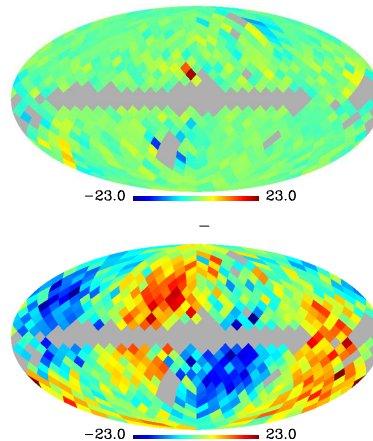


**Figure 5.** Downgraded (to  $N_{side} = 8$ ) Q1-band difference maps in Galactic coordinates and in units of  $\mu\text{K}$ . The gray area represents pixels without valid value. *Upper panel:* the map produced with our map-making software from the TOD used to make the published WMAP5 year-1 map minus the corresponding safe-mode map. *Lower panel:* The WMAP5 year-1 official map minus the corresponding safe-mode map.

and accurate. If the final power spectrum is consistent with the input  $\Lambda\text{CDM}$  power spectrum, then we can say that our entire data processing has been tested for all aspects and been well justified.

We give the results of this test in Fig. 4. More than 99% of  $C_{final} - C_{\Lambda\text{CDM}}$  is attributed to the random fluctuation introduced automatically by synfast to simulate the cosmic variance. To isolate and show the tiny error attributed to the overall map-making and power spectrum estimation processes, we derive cross power spectrum from the V and W-bands maps generated by synfast ( $C_{synfast}$ ) with the same power spectrum estimation program and compare  $C_{final}$  with  $C_{synfast}$  in the lower panel of Fig. 4. This is the true variation introduced by the overall map-making and power spectrum estimation processes.

For  $l = 2 - 700$ , the average is only  $0.0052 \mu\text{K}^2$  and rms only  $0.51 \mu\text{K}^2$  for  $C_{final} - C_{synfast}$ , the average is only  $-6.49 \mu\text{K}^2$  and rms is  $234.96 \mu\text{K}^2$  for  $C_{final} - C_{\Lambda\text{CDM}}$ . Therefore, we see no systematical bias in either  $C_{final} - C_{synfast}$  or  $C_{final} - C_{\Lambda\text{CDM}}$ , and the overall map-making and power spectrum estimation has high accuracy. In other words, our map-making and power spectrum estimation has passed the end-to-end test and has been well justified.

The correlation maps of residual TOD shown in §3.1 demonstrate that our map-making product is consistent with the input TOD, but the published WMAP maps contain remarkable constructed error component produced during map-making. The results of testing residual dipole component amplitude (§3.2) and convergence of iterative map-making algorithm (§3.3) show that our software has good performance. The end-to-end simulations (§3.4) give a prove that all our data pipeline is comprehensively self-consistent. We therefore expect the temperature map recovered from WMAP TOD by our software can provide more reliable result for CMB study.

It is worth to note that, with our map-making program, we also reconstruct temperature maps from the TOD used to produce the released WMAP5 map. We find that, despite a few minor differences, the obtained map is much more consistent with our safe-mode map than with the WMAP team’s official map, as presented in Fig. 5,

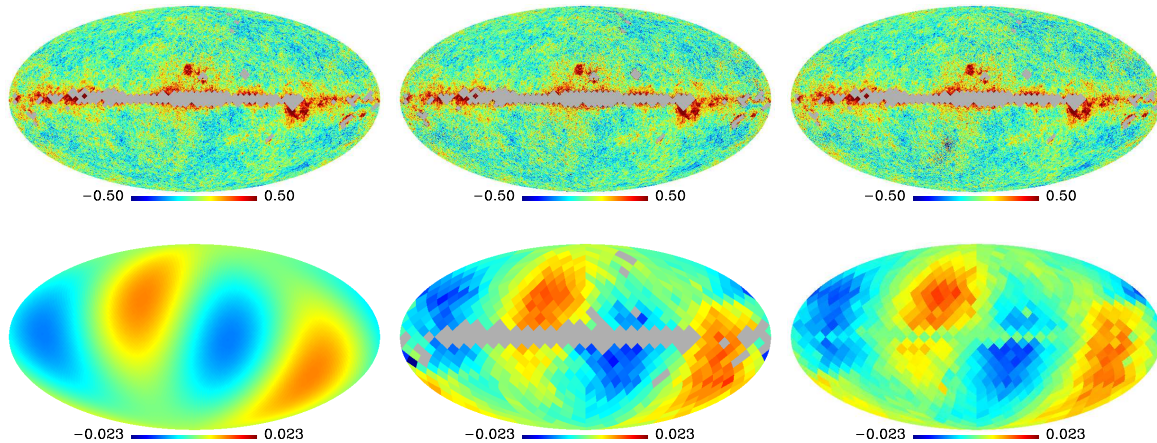


**Figure 6.** **Upper panel** – Q1-band temperature maps in units of mK and in Galactic coordinates. The monopole and dipole components have been removed for all maps. *From left to right*: the official WMAP5 map; the new WMAP5 map reconstructed from the TOD used in WMAP5 map-making but by our software; the safe-mode map reconstructed from high quality WMAP5 TOD by our software. **Lower panel** – *Left*: the quadrupole component of the official WMAP5 CMB map; *Middle*: the difference between the official WMAP5 map and the new WMAP5 map (smoothed to  $N_{side} = 8$ ); *Right*: the difference between the official WMAP5 CMB map and the safe-mode map (smoothed to  $N_{side} = 8$ ).

which illustrates the safe-mode being not the reason of the major difference between the WMAP release and our result.

#### 4 TEMPERATURE MAPS

With our map-making software we reconstruct sky temperature maps from WMAP TOD. In this work we discuss and solve for the temperature only, which is the average of all four WMAP channels:  $d = (d_{13} + d_{14} + d_{23} + d_{24})/4$ . The final temperature maps are derived from TOD with 80 rounds of iterations. The map-making is done in  $N_{side} = 512$  resolution (Gorski et al. 2005) and the HEALPix nested pixelization scheme only. Observations that have either beam inside the WMAP5 processing mask are rejected in our map-making, hence all pixels inside the WMAP5 processing mask have no values in the final temperature map. However, this does not affect the power spectrum estimation, because the WMAP5 processing mask is completely covered by the mask used for power spectrum estimation (the KQ85 mask or the enlarged KQ85 mask, which is discussed in §5.1), the pixels with no values will not be introduced into the power spectrum estimation.

The upper-left plot of Fig. 6 is the WMAP5 official release for the Q1-band, and the upper-middle plot shows the new CMB temperature map of the Q1-band derived from the WMAP5 used TOD by our map-making software (both have the best-fit dipole and monopole components removed, and the plotted temperature ranges are  $-0.5 - 0.5$  mK). The differences between them (official WMAP5 map minus our map) are computed. We downgrade the difference map to a low resolution map with the resolution parameter  $N_{side} = 8$  and show in the lower-middle plot of Fig. 6.

The rms temperature fluctuation on the smoothed difference map in the lower-middle plot of Fig. 6 is  $6.6 \mu\text{K}$ , which is much higher than all known map making errors. We notice that, the downgraded difference map in the lower-middle plot of Fig. 6 is almost the same with the WMAP5 quadruple component (lower-left of Fig. 6), which indicates the quadruple component in the WMAP5 CMB map is almost completely artificial.

We also reconstruct a safe-mode map from the WMAP5 Q1-

band TOD of safe-mode by our map-making software and compute its difference to the official WMAP5 map, the results, shown in the upper-right and lower-right plots of Fig. 6 respectively, are very similar to what produced from the WMAP5 used TOD, demonstrate again the observed remarkable difference is mainly produced by the WMAP map-making process.

#### 5 CMB ANGULAR POWER SPECTRUM

##### 5.1 Estimation Method

To produce a reliable CMB power spectrum, the foreground emission should first be subtracted from a raw temperature map to make the clean CMB temperature map. Our single-year clean maps are produced with the foreground removal technique used by the WMAP team (Hinshaw et al. 2007; Gold et al. 2009), then the best-fit dipole and monopole components are subtracted before power spectrum estimation. After these operations, 30 V and W-bands single-year temperature maps are used to compute 435 cross power spectra with the KQ85 mask (same as WMAP team’s five-year cross power spectra estimation scheme). For the safe-mode maps, due to data rejection pixels in some areas of the single-year maps contain no usable observation. To exclude these pixels (as well as pixels with too few observations) in computing the CMB power spectra, an extra mask that mainly lies on the ecliptic plane is used in addition to the KQ85 mask (which is the default mask for WMAP team’s power spectrum estimation) to constitute an enlarged KQ85 mask as shown in Fig. 7.

The released WMAP CMB power spectrum is derived from temperature maps via several main steps including the cross-power spectrum estimation, cut-sky correction, beam function correction, and pixel window correction (Hinshaw et al. 2003b). Two software packages, HEALPix and PolSpice, are designed to do these (Gorski et al. 2005; Szapudi et al. 2001; Chon et al. 2004). The main difference between them is that HEALPix does not support the cut-sky correction directly, but PolSpice does. Therefore, we use PolSpice in this work to produce power spectra from our single-year maps. HEALPix are also used with the cut-sky correc-

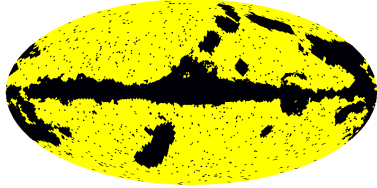


**Figure 7.** The enlarged KQ85 mask used in computing single year cross-power spectra.

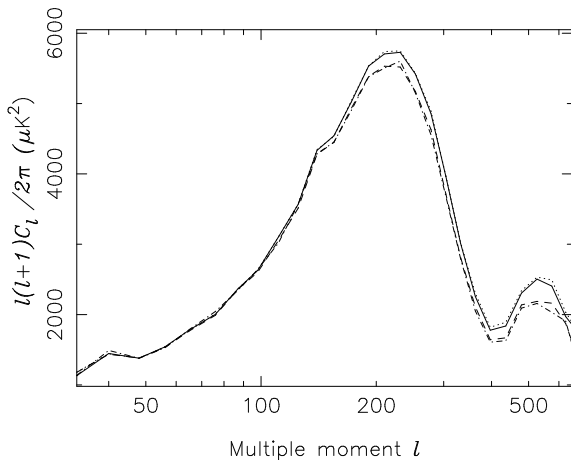


**Figure 8.** Binned cross-power spectra ( $l = 33 - 675$ ). *Solid line*: the released WMAP5 spectrum. *Dotted line*: the spectrum derived by us from released WMAP5 maps to test our power spectrum estimation processes (very close to the solid line and is hard to distinguish). *Dashed line*: the spectrum of new CMB maps from WMAP5 used TOD and our map-making software. *Dashed-dotted line*: the spectrum of safe-mode CMB maps from WMAP5 safe-mode TOD and our map-making software.

tions done by our own software, and the results are almost identical with PolSpice results.

## 5.2 Power Spectrum

For a start, to test our power spectrum estimation processes, we derive a binned power spectrum from the released WMAP5 CMB maps with the same binning scheme as the WMAP team used. The obtained spectrum is nearly identical with what provided by the WMAP team (see the solid line and dotted line in Fig. 8, where the two WMAP5 power spectra obtained by the WMAP team and by us respectively are so close to each other that it is hard to distinguish them). Then we compute the binned cross power spectrum from our new CMB maps with WMAP5 used TOD and that with WMAP5 safe-mode TOD respectively, the results are shown in Fig. 8 for high order moments ( $l = 33 - 675$ ) and Fig. 10 for low order moments ( $l < 30$ ) respectively.

We also compute binned cross-power spectra from raw maps before foreground subtraction for WMAP5 release and for our safe-mode maps separately, the results are shown in Fig. 9. From Fig. 9 we can see that the remarkable difference between the official and our new spectra does not come from the foreground removal process.

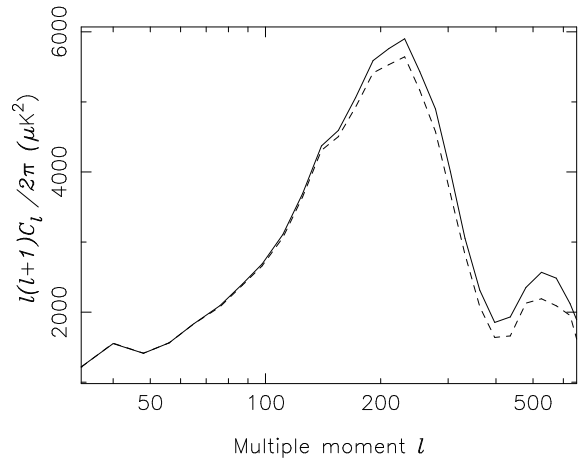


**Figure 9.** Binned cross-power spectra from raw maps before foreground subtraction. *Solid line*: from the released WMAP5 maps. *Dashed line*: from our safe-mode maps.

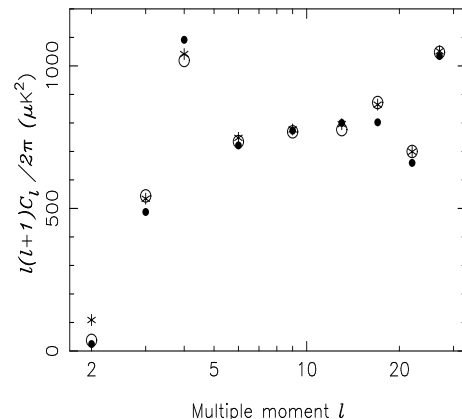


**Figure 10.** Low- $l$  cross-power spectra ( $l < 30$ ). *Asterisk*: the released WMAP5 spectrum. *Circle*: the spectrum of new CMB maps from WMAP5 used TOD and our map-making software. *Filled circle*: the spectrum of safe-mode CMB maps from WMAP5 safe-mode TOD and our map-making software.

## 5.3 Low Order Moments

Fig. 10 shows large-scale binned CMB power spectra for multiple moment  $l < 30$ , where asterisks mark WMAP5 release, circles and filled circles mark our results from new WMAP5 maps and safe-mode maps respectively.

The remarkable quadruple structure in the difference map reminds us to see whether the large scale anomalies detected in the released WMAP CMB power spectrum are really cosmic origin or just an observation effect for some artificial reasons. A lack of anisotropy power on the largest angular scales has long been observed in WMAP CMB maps (Bennett et al. 2003b; Hinshaw et al. 2003b; Hinshaw et al. 2009). We see from Fig. 10 that the power at  $l = 2$  further drops to nearly zero in our CMB maps ( $37.3 \mu\text{K}^2$  from our new WMAP5 maps,  $24.4 \mu\text{K}^2$  from our safe-mode maps, vs.  $108.7 \mu\text{K}^2$  from WMAP5 release)<sup>2</sup>; meanwhile, the power spectrum uncertainty attributed to measurement

<sup>2</sup> The WMAP5 power spectrum and our power spectrum here are the pseudo- $C_l$  based cross power spectrum.

Table 1: Average power spectrum ( $\mu\text{K}^2$ )

L	WMAP5	BOOMRANG <sup>1</sup>	This work
220	5716(+2.8%)	5558(reference)	5554(-0.1%)
500-600	2454	2308	2095
800-950	2427(+36%)	1783(reference)	1766(-1%)
220-950	2584	2367	2174

<sup>1</sup> arithmetic average of BOOMRANG98 and 03

errors at  $l = 2$  is  $\sim 5.60 \mu\text{K}^2$  only<sup>3</sup>. The quadrupole component ( $l = 2$ ) drops for nearly 78% from the WMAP5 value, whereas the power differences between the WMAP5 and our spectra at other multiple moments in Fig. 10 are all  $< 10\%$ . It seems unlikely that a nearly zero power spectrum at  $l = 2$  can be covered by the cosmic variance.

The unexplained orientation of large-scale patterns of CMB maps in respect to the ecliptic frame has long puzzled cosmologists. By analyzing CMB maps from the first year WMAP data, Tegmark et al. (2003) found both the CMB quadrupole ( $l = 2$ ) and octopole ( $l = 3$ ) having power along a particular spatial axis, and more works (de Oliveira-Costa et al. 2004; Eriksen et al. 2004; Schwarz et al. 2004; Jaffe et al. 2005) found that the preferred directions of these two low- $l$  components are highly aligned and close to the ecliptic plane. Recently, significant signal spatially correlated with the ecliptic plane was detected by Diego et al. (2009) in published WMAP5 map and by Jiang, Lieu and Zhang (2009) from analyzing spectral variation. In our maps, the unexplained quadrupole-octopole alignment disappears: in the WMAP5 release, the angles between the preferred directions of CMB quadrupole and octopole average out at  $6^\circ.5$  for all 30 single year maps; whereas our single year maps give  $26^\circ.1$  average angle between the two components. Fig. 11 compares the quadrupole and octopole components averaged over 30 V and W bands our single-year maps and the corresponding WMAP5 maps results directly. We can see that both the direction and amplitude of the quadrupole component have changed significantly from the WMAP5 official maps to our new maps.

#### 5.4 High Order Moments

Fig. 8 shows the binned cross power spectra for high order moments ( $l = 33 - 675$ ), where the solid line is the released WMAP5 spectrum, the dashed line the spectrum of new CMB maps from WMAP5 used TOD and our map-making software, and the dashed-dotted line the spectrum of safe-mode CMB maps from WMAP5 safe-mode TOD and our map-making software. From Fig. 8 we see the new power spectra being systematically lower than the released WMAP5 power spectrum over multiple moment  $l = 200 - 675$ . For example, by averaging all the power spectra in this range, both HEALPix and PolSpice give our safe-mode power spectrum being averagely 13% lower than WMAP5. Such a power spectrum decrease will cause important consequences on the best fit cosmological parameters.

It is interesting to see from Table 1 that, in comparison with

<sup>3</sup> The WMAP5 power spectrum uncertainty at  $l = 2$  consists of the measurement errors and the cosmic variance. The later is dominating, but it has nothing to do with map making or power spectrum estimation uncertainties. Therefore, we don't have to discuss it here.

the WMAP release, new power spectra in high order moment region are, in general, better consistent with the BOOMRANG CMB spectrum (Ruhl et al. 2003; Jones et al. 2006). Especially for the power spectrum near the third peak ( $L=800-950$ ). The relative deviation from the BOOMRANG spectrum at the first peak ( $l = 220$ ) is  $\sim 3\%$  for WMAP5 and only  $\sim 0.1\%$  for our safe-mode spectrum respectively; at the third peak ( $l = 800 - 950$ ), that is  $\sim 36\%$  for WMAP5 and only  $\sim 1\%$  for our spectrum, respectively.

## 6 COSMOLOGICAL PARAMETERS

The peak height ratio (first peak/second peak, which is closely related to the baryon density) in the CMB power spectrum is  $\sim 2.2$  for WMAP5 release and  $\sim 2.6$  for our spectrum, indicating that at least the baryon density should rise. To roughly estimate to what extent the cosmological parameters can be affected, a brutal force least-square fit search for the new best-fit parameters is done in the multiple moment range from 33 to 675 by using the CMB-Fast package (Zaldarriaga et al. 1998; Zaldarriaga & Seljak 2000; Seljak et al. 1996) with the  $\Lambda$ CDM model for our new WMAP5 binned power spectrum and safe-mode spectrum separately. The two sets of results are close to each other. The results from the safe-mode spectrum are listed in Table 2. From Fig. 8, we can see the new power spectrum differs by no more than 20% from the WMAP5 power spectrum. Therefore, the WMAP5 uncertainties of the cosmological parameters are roughly suitable for the new cosmological parameters, as adopted in Table 2.

From Table 2 we can see that, in comparison with the WMAP5 release, some best-fit cosmological parameters from the improved CMB maps are significantly different, e.g. the total matter density  $\Omega_m = \Omega_c + \Omega_b$  increases by  $\sim 25\%$  (from 0.26 up to 0.32) and the dark energy density  $\Omega_\Lambda$  decreases by  $\sim 10\%$  (from 0.74 down to 0.68).

## 7 DISCUSSION

In this work we observe remarkably systematic artifacts in the released WMAP CMB map, structured signals and noises related with the Solar System, as shown by Fig. 1, Fig. 5 and Fig. 6, which turn into the almost all observed quadrupole component of the released map. From Fig. 11 we can see that the detected ecliptic contamination mostly comes from the map-making process of the official WMAP temperature map, the non-zero flagged TOD used by the WMAP team in their map-making are the secondary source. It will be very helpful if the WMAP team can thoroughly recheck their map-making process to find out where and how the error occurs, because it is difficult to do so for a non-WMAP team member.

In this work, we built a self-consistent software package of map-making from TOD and power spectrum estimation from recovered CMB map. Our software successfully passes through a variety of tests. With the tested software we reconstruct new CMB maps from WMAP TOD, which are significantly different with the official WMAP maps. Our map-making process prevent the problem of inconsistency between input TOD and reconstructed map: the anomaly structure and high fluctuation observed in the residual TOD of official WMAP maps disappear in the residual TOD of our new maps. Therefore, the new CMB maps are certainly improved by our map-making and more reliable than the WMAP release.

The difference between the old and new temperature maps is almost the same with the quadrupole component of the released

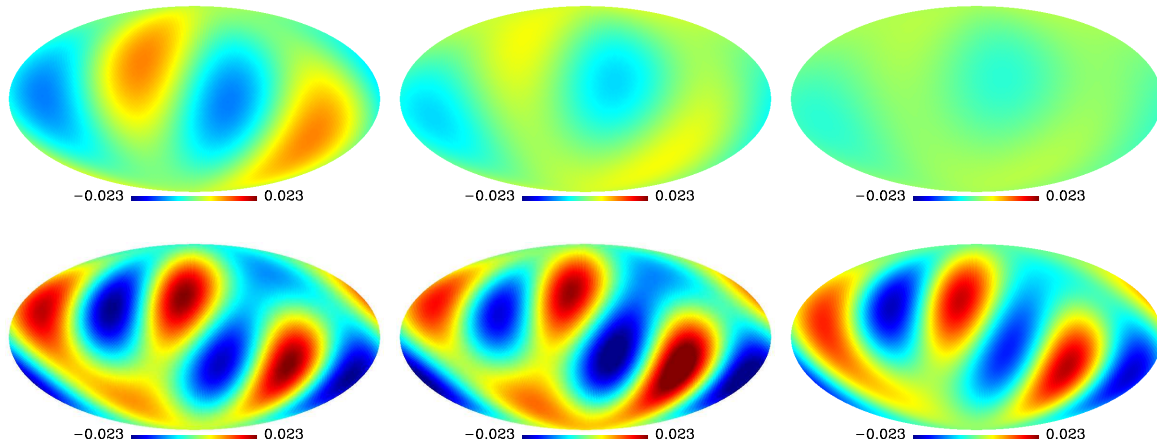


**Figure 11.** Quadrupole (upper panel) and octopole (lower panel) components averaged among 30 V and W bands single-year maps. From left to right: WMAP5 release, from new maps reconstructed with WMAP5 used TOD and our map-making software, from our safe-mode CMB maps.

Table 2: The best-fit cosmological parameters

Description	Symbol	Value		
		WMAP5-only <sup>1</sup>	WMAP5+BAO+SN <sup>1</sup>	This work
Hubble constant (km/s/Mpc)	$H_0$	$71.9^{+2.6}_{-2.7}$	$70.1 \pm 1.3$	$71.0 \pm 2.7$
Baryon density	$\Omega_b$	$0.0441 \pm 0.0030$	$0.0462 \pm 0.0015$	$0.052 \pm 0.0030$
Dark matter density	$\Omega_c$	$0.214 \pm 0.027$	$0.233 \pm 0.013$	$0.270 \pm 0.027$
Dark energy density	$\Omega_\Lambda$	$0.742 \pm 0.030$	$0.721 \pm 0.015$	$0.678 \pm 0.030$
Fluc. Ampl. at $8h^{-1}$ Mpc	$\sigma_8$	$0.796 \pm 0.036$	$0.817 \pm 0.026$	$0.921 \pm 0.036$
Scalar spectral index	$n_s$	$0.963^{+0.014}_{-0.015}$	$0.960^{+0.014}_{-0.013}$	$0.957 \pm 0.015$
Reionization optical depth	$\tau$	$0.087 \pm 0.017$	$0.084 \pm 0.016$	$0.109 \pm 0.017$

<sup>1</sup> from Hinshaw et al. (2008)

WMAP5 CMB map (Fig. 6). Being consistent with this, we also see a structure similar to the released WMAP5 quadrupole component after smoothing the map of the WMAP residual TOD (Fig. 1) to  $N_{side} = 8$ . The correlation map of the residuals between input TOD and predicted by the released WMAP temperature map is also very similar to the quadrupole component observed in the released WMAP CMB map. Such phenomenon strongly suggests that, in the WMAP5 CMB temperature map, a very large portion of the presently known quadrupole component is actually artificial. As a natural consequence, in our new CMB map the  $l = 2$  fluctuation falling near the ecliptic plane no longer exists, and then the quadrupole component is nearly zero.

Despite cosmic variance, the anisotropy at the lowest harmonics as inferred from our reprocessed sky maps are likely to be too low to accommodate the standard cosmological parameters. A nearly zero quadrupole component of CMB map places a tight constraint on the nature of the early universe. As well known, the subtended angle of the cosmological horizon at last scattering is only about 1 - 2 degree. Measured CMB power at the large angular scale of lowest moments should reflect the circumstance of the inflation period, e.g. the state of matter and the production of density fluctuations during inflation. Our result indicates that we may catch sight of the very early rigid universe, the primordial density perturbations should be generated in a later stage of inflation. It is hopeful to study the generation and revolution of density fluctuation through

more reliable large scale CMB data and with suitable mathematical tool for data analysis in the future.

Besides the ecliptic foreground contamination revealed in this work, we have found other two kinds of systematic distortions in official WMAP maps. One is the Galactic foreground contamination. Although the WMAP team has paid huge attention to separate the temperature anisotropy of CMB from Galactic foreground emission, in released WMAP CMB maps we still find notable distortion from hot Galactic sources (Liu & Li 2009): pixels  $141^\circ$  away from the hottest pixels in the Galactic plane are on average  $12 - 14 \mu\text{K}$  cooler than average pixels. Another one is the non-negligible effect of imbalance WMAP observations (Li et al 2009): significant correlation between the map temperature released by the WMAP team and the difference in the observation numbers that a pixel is pointed by the satellite's two antennae, the temperature distortion caused by this observational effect is as high as up to  $\sim 20 \mu\text{K}$ . These two kinds of systematics are also detected in our new maps and should be further inspected and corrected. Therefore we believe that there still exist space to improve CMB maps and accuracies of cosmological parameters again by further improving map-making from WMAP TOD data and removing residual systematic errors in recovered temperature maps.

Except the quadrupole component, the power differences between the WMAP5 and our low- $l$  spectra at other multiple moments (Fig. 10) are not too large. The anomalously planar cosmic octopole still remains in our new WMAP5 CMB map, and also in



the safe-mode map just with a little lower amplitude (see Fig. 10 and Fig. 11). However, from our recent analysis, we find that the effect of imbalance WMAP observations may contribute to some extent to the observed octopole component in WMAP CMB maps, and the real spectrum at  $l = 3$  might be lower than observed. It is expected that more reliable low- $l$  spectrum can be derived after better understanding and properly correcting systematics in observation and problems in map-making. A reliable large-scale spectrum will certainly help to understand the early universe. For example, for the primordial density perturbations, inflation theory predicts the index  $n$  in the scalar spectrum  $P(k) \sim k^n$  being nearly unit,  $n \approx 1$ , over a very wide range of  $k$  by virtue of scale invariance: most perturbations exited the horizon with the same amplitude in the brief interval of rapid exponential expansion. There is now a possibility that a larger  $n$  at low  $l$  might be more consistent with the data. This in turn would mean that quantum fluctuations generated during inflation may no longer be a viable source of super-horizon perturbations without significant modification.

The best fit cosmological parameters of this work shown in Table 2 are just preliminary results. It is interesting that, for nearly all the basic cosmological parameters ( $H_0$ ,  $\Omega_b$ ,  $\Omega_c$ ,  $\Omega_\Lambda$ ,  $\sigma_8$ ,  $n_s$ ), both our values and the WMAP + BAO + SN cosmological parameter values (Hinshaw et al. 2009) are simultaneously higher or lower than the WMAP5 alone (Hinshaw et al. 2009). This shows that the new cosmological parameters given by us (although still rough) match with improved accuracy those of other two different kinds of measurements: the distance measurements from the Type Ia supernovae (SN) and the Baryon Acoustic Oscillations (BAO) in the distribution of galaxies.

## ACKNOWLEDGEMENTS

Prof. Richard Lieu, Tan Lu, Miao Li, Xinmin Zhang, Charling Tao and the anonymous referee are thanked for helpful comments and suggestions. This work is supported by the National Natural Science Foundation of China (Grant No. 10533020) and the National Basic Research Program of China (Grant No. 2009CB-824800). The data analysis made use of the WMAP data archive and the HEALPix, PolSpice, CMBFast software packages.

## REFERENCES

Aurich, R., Lustig, S. & Steiner, F., 2009, arXiv:0903.3133  
 Bennett, C.L. et al., 2003, ApJ, 583, 1  
 Bennett, C.L. et al., 2003, ApJS, 148, 1  
 Chon, G. et al., 2004, MNRAS, 350, 914  
 de Oliveira-Costa, A., Tegmark, M., Zaldarriaga, M. & Hamilton, A., 2004, Phys. Rev. D, 69, 063516  
 Diego, J. M., Cruz, M., Gonzalez-Nuevo, J., Maris, M., Ascasibar, Y. & Burigana, C. 2009, MNRAS, submitted; arXiv:0901.4344  
 Eriksen, H.K., Hansen, F.K., Banday, A.J., Grski, K.M. & Lilje, P.B., 2004, ApJ, 605, 14  
 Gold, B. et al., 2009, ApJS, 180, 265  
 Gorski, K. et al., 2005, ApJ, 622, 759  
 Hill, R. S., et al. 2009, ApJS, 180, 246  
 Hinshaw, G. et al., 2003a, ApJS, 148, 63  
 Hinshaw, G. et al., 2003b, ApJS, 148, 135  
 Hinshaw, G. et al., 2007, ApJS, 170, 288  
 Hinshaw, G. et al., 2009, ApJS, 180, 225

Jaffe, T.R., Banday, A.J., Eriksen, H.K., Grski, K.M. & Hansen, F.K., 2005, ApJ, 629, L1  
 Jarosik, N. et al., 2007, ApJS, 170, 263  
 Jiang, B.Z., Lieu, R. & Zhang, S.N., 2009, ApJ, submitted; arXiv:0904.2513  
 Jones W. C., et al., 2006, ApJ, 647, 823  
 Limon, M. et al., 2008, *Wilkinson Microwave Anisotropy Probe (WMAP) : The Five-Year Explanatory Supplement*, Greenbelt, MD: NASA/GSFC; Available in electronic form at <http://lambda.gsfc.nasa.gov>  
 Li, T.P., Liu H., Song L.M., Xiong S.L. & Nie J.Y., 2009, MN-RAS, 398, 47  
 Liu, H. & Li, T.P., 2009, Sci China G-Phy Mech Astron, 52, 804; arXiv:0809.4160v2  
 Ruhl, J.E., et al., 2003, ApJ, 599, 786  
 Schwarz, D.J., Starkman, G.D., Huterer, D. & Copi, C.J., 2004, Phys. Rev. Lett., 93, 221301  
 Seljak, U. & Zaldarriaga, M., ApJ, 1996, 469, 437  
 Szapudi, I. et al., 2001, ApJ, 548, L115  
 Tegmark, M., de Oliveira-Costa, A. & Hamilton, A.J., 2003, Phys. Rev. D, 68, 123523  
 Zaldarriaga, M., Seljak, U. & Bertschinger, E., 1998, ApJ, 494, 491  
 Zaldarriaga, M. & Seljak, U., 2000, ApJS, 129, 431